Chapter 2

The SMART and *"all" the relevant techniques*

Before the SMART microscope is described, there will be a short introduction to the development of aberration corrected LEEM/PEEM instruments.

2.1 A brief history of aberration-corrected microscopy

The first PEEM experiments have been reported by *E. Brüche et al.* [10] and date back to the early 1930s. The technological development of the instruments has improved since then under many aspects from vacuum quality to lateral resolution. It took only a few years until a theoretical limitation to the resolution of PEEMs and LEEMs was proposed in what is known as *Scherzer's* theorem [11], which states that:

> *The chromatic and spherical aberrations of an electron microscope with round lenses, real images, static fields, no space charge and a potential and it's derivative without discontinuities, are always positive.*

The resolution limit of the above is dominated by the chromatic and spherical aberrations resulting from the objective lens. The objective used in such microscopes is known as a *cathode lense*. The reason for this terminology is that a medium range base

potential E (of 15–18 kV) is used to accelerate the electrons emitted at a start energy E_0 at the sample surface to a final kinetic energy of $E + E_0$.

Other image deterioration effects, such as astigmatism mainly results from misalignment or from constructional limitations and can be compensated by stigmators. Coma and distortions of the field are normally of minor importance. We now derive the relation between resolution and aberration coefficients following the discussion as in *Schmidt et al.* [12]. The resolution is given by

$$d = \sqrt{d_\mathrm{d}^2 + (d_\mathrm{s}/2)^2 + d_\mathrm{c}^2} \tag{2.1}$$

where d_s and d_c are the radii of the disks of confusion due to the spherical and chromatic aberrations of the lens with:

$$d_\mathrm{s} = C_\mathrm{s} \sin^3 \alpha \tag{2.2}$$

$$d_\mathrm{c} = C_\mathrm{c} \frac{\Delta E}{E_0} \sin \alpha \tag{2.3}$$

The radius of the confusion spot due to the diffraction at the smallest aperture is:

$$d_\mathrm{d} = 0.61\, \lambda / \sin \alpha \tag{2.4}$$

α is the acceptance angle or the maximum emission angle contributing to the image. The parameters C_s and C_c depend on the lens adopted and the start energy E_0 and base energy E. The dependance of the resolution on the emission angle α, with realistic C_s and C_c calculated by [6], is plotted in figure 2.1. Mainly two contributions limit the highest resolution obtainable. At values of α lower then $\sim$ 20 mrad the resolution is said to be diffraction limited, while at higher values it is dominated by the chromatic aberrations. The spherical aberrations come into play at values of α higher than $\sim$ 400 mrad. The specific uncorrected maximum resolution obtainable is of about $\sim$ 15 nm.

This is clearly not satisfactory for the investigation of objects with dimensions below $\sim$ 5 nm. The constraints mentioned in *Scherzer's* theorem can be circumvented in different ways. These are listed in table 2.1. Some methods were already proposed by *Scherzer*, but the technological development was too demanding from the computational and experimental point of view.

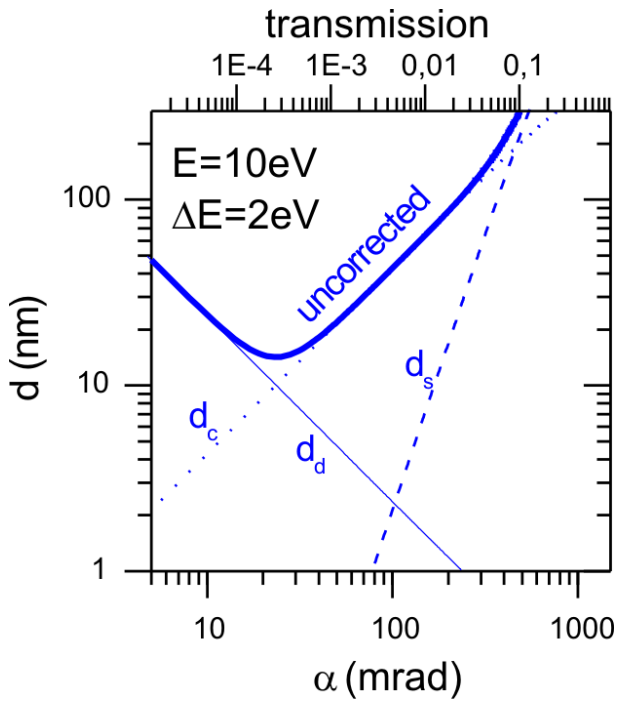

Figure 2.1: Resolution limit d of a function of acceptance angle α for an uncorrected objective lens. The thin dashed and dotted lines represent the single aberration terms (figure adapted from [12]).

Nowadays, TEM can already correct the spherical aberrations (which are dominant at the high energies of $\sim$ 200 keV) and have proven lateral resolutions below 1 Å [22, 23]. The aberrations of scanning electron microscopes have been corrected, both spherical and chromatic. The development in PEEM and LEEM has been slower. The chromatic aberrations have been proven to be corrected in 2002 by *Schönhense* and *Spiecker* [21] by means of a pulsed source and pulsed electric fields. In 2005 *Koshikawa et al.* were able to correct both, spherical and chromatic aberrations, with a method known as moving focus [24]. Both methods however are technically very demanding and with strong limitations. Using a pulsed source and a switching electrical field in the projector lens, *Schönhense* and *Spiecker*, were able to correct *only* chromatic aberrations. This is critical for the imaging of electrons with kinetic energies above $\sim$ 100 eV where the spherical aberrations start to be the dominating contribution to the final intensity (see figure 1 in [12]). However, the correction of spherical aberration appears to be beyond our technical capabilities. Furthermore, no improvement of resolution was

Table 2.1: Known aberration correction methods.

Method	Correction	Precondition broken	Ref.
EM combination of quadrupoles	C_c	non-round sym.	[13]
Wien filter	C_c	non-round sym.	[14]
EM combination of quadrupoles and octupoles	C_s	non-round sym.	[13]
Hexapole-doublet	C_s	non-round sym.	[15]
Microwave-excited lens systems	$C_c + C_s$	non-static field	[16, 17]
Moving focus method	$C_c + C_s$	non-static field	[18, 19].
Grids and foils	$C_c + C_s$	charge	[20].
Time structure of pulsed excitation sources	$C_c + C_s$	non-static field	[21]
Electron mirror	$C_c + C_s$	virtual images	[5, 6]

demonstrated, the intensity obtained of the obtained images is poor and no beam splitter can be implemented to image reflected electrons (LEEM).

The correction of aberrations with the *moving focus* method has also some drawbacks: (i) the brightness of the Hg-short arc lamp had to be improved by a factor 100 with respect to commercial instruments, (ii) even though the range of moving focus depends on the spherical aberration coefficient C_s *after* acceleration of the electrons, there is no clear relationship between C_s before and after acceleration (iii) for *one* aberration corrected image, 41 single images, with an acquisition time of 10 sec, had to be superimposed (almost 7 min). The obtained final lateral resolution was 12.5 nm (which is still not below the theoretical lateral resolution of ~ 10 nm).

The use of a mirror has many advantages. Figure 2.2 shows how the resolution can be improved using an electron tetrode mirror. Besides a theoretical increase in lateral resolution from approx. 15 nm to below 2 nm, the transmission of the instrument can be increased, due to use of a larger acceptance angle, of approx. a factor 100. This is the only aberration correction method, for both C_s and C_c, that does not require any superposition of images or time structured excitation sources. It is therefore possible

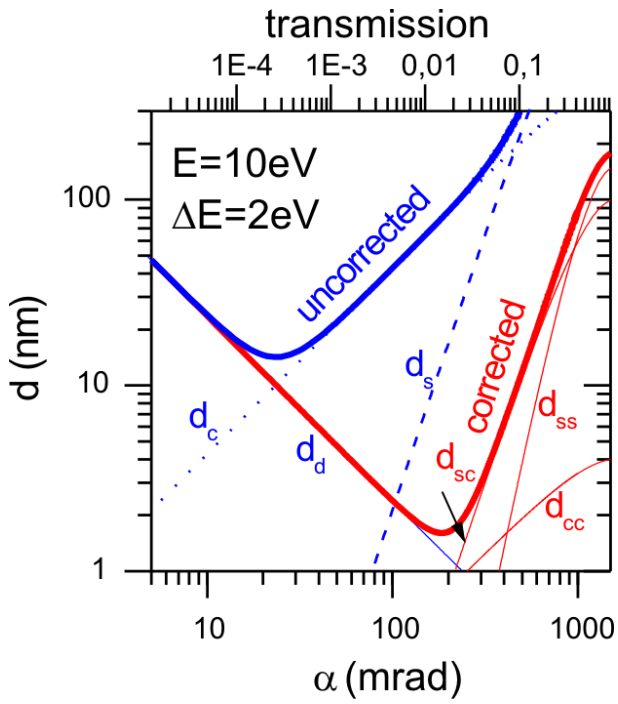

Figure 2.2: Resolution limit d of an corrected and uncorrected objective lens (red and blue lines respectively) as a function of acceptance angle α. The thin lines represent the dominating aberration terms (figure adapted from [12]).

to use the microscope as a conventional non-aberration corrected instrument without being limited by long image acquisition periods and the time structure of the excitation source (in this case all the potentials are static).

In the following of the section the SMART spectro-microscope is presented. First a general overview of how the whole spectro-microscope works is given in paragraph 2.2. then the details of some of the microscope's building blocks are discussed in a more comprehensive way in the following paragraph 2.3. In the appendix an example of how the alignment procedure works, peculiar for this instrument and necessary for high resolution imaging, is shown.

2.2 The Spectro-Microscope

The outline of the microscope components is shown in figure 2.3. The building blocks of the system, and which group of the cooperation constructed them, is given in the following[1]:

1. the main chamber[(a)] and sample manipulator[(b)],
2. the preparation chamber is adapted for quick sample exchange[(a)],
3. the electron gun[(e)] and illumination optics[(d)],
4. the aberration corrector/mirror[(c)],
5. the magnetic beam separator or beam splitter[(c)] with deflection angles of 90°,
6. the imaging column[(d)],
7. the energy analyzer, commonly referred to as omega-filter[(d)],
8. the projection optics[(d)] with the 2d-detector[(b)],
9. the refocussing mirror for the soft X-ray illumination[(a–f)].

The instrument is mounted on a frame with vibration damping[(d)].

The microscope, which is the topic of this thesis, is located at the BESSY II synchrotron in Berlin. From the beamline monochromatized photons in the energy range between 90 and 2000 eV are used for the excitation of electrons and are focused to an area of about 6 μm by 30 μm. Alternatively another source for photoelectrons is a laboratory UV-light source whose maximum photon energy is in the range of 4.9 eV. These two photon sources allow two microscopic modes, among others, known as X-ray PhotoElectron Emission Microscopy (X-PEEM) and Ultra-Violet PhotoElectron Emission Microscopy (UV-PEEM), respectively.

[1]The following cooperation partners have contributed: (a) Universität Würzburg, (b) TU Clausthal, (c) TH Darmstadt, (d) Fritz-Haber-Institut der Max-Planck-Gesellschaft, (e) LEO Elektronenmikroskopie GmbH, (f) BESSY.

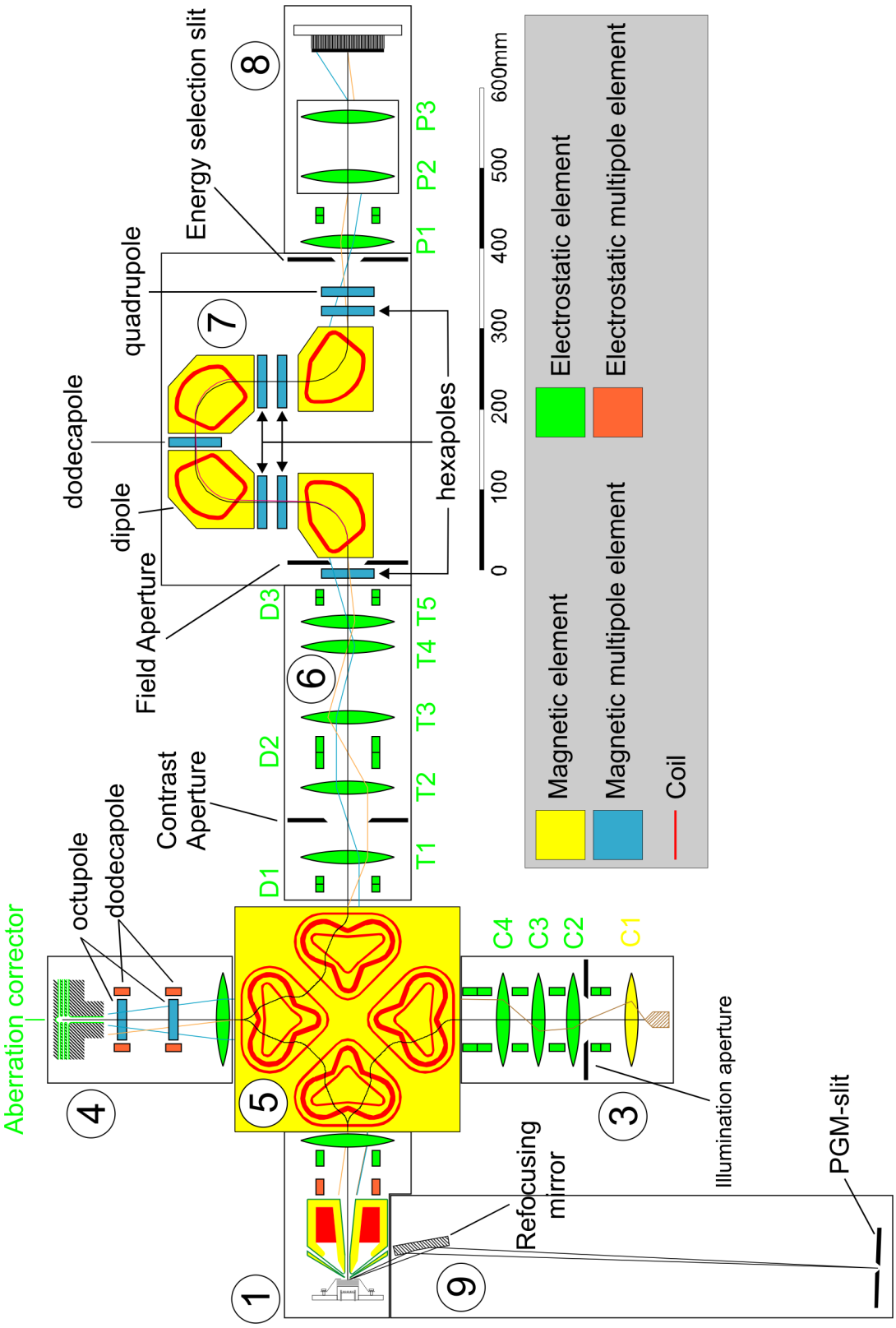

Figure 2.3: Schematic overview of the microscope.

As a third method, the sample can be illuminated with electrons extracted from a cold-cathode field emitter and lead through the beamsplitter. Then the reflected electrons are used for imaging. In this case the microscopic mode is Low Energy Electron Microscopy (LEEM).

In all cases, the photoemitted or reflected electrons are then accelerated to 15 keV of energy with the immersion electromagnetic lens. The sample-lens distance (often referred to as working distance) is 2 mm, resulting in an electrical field at the sample surface of $7.5 \cdot 10^6$ V/m. The electric field at the sample surface can eventually be reduced, if necessary down to zero, by introduction of an intermediate electrode (to this date, this has not been implemented). The magnification of the image due to the passage through the objective lens, resulting from a combination of electric and magnetic fields, is in the range between 18 and 26 times and depends on the start voltage. The focus of the field lens between objective lens and beam splitter is located in the back focal plane of the objective lens so that the paraxial field rays run parallel at the entrance of the beam splitter. This is an essential requirement of the beam splitter: the image plane has to be at the entrance and the back focal plane at infinity. The same situation is reproduced at the exit plane (magnification 1) after a 90° deflection, without introducing second order aberrations or dispersions of first or second order.

The tetrode mirror, combined with the mirror field lens, reflects back the rays to reform an intermediate image at the entrance of the beam splitter without magnifying it (magnification = 1). Spherical and chromatic aberrations are introduced in the image, by appropriate tuning of three of the four electrode potentials of the mirror (the fourth electrode is at ground potential). They are of the opposite sign of those generated by the objective lens. Between the mirror and the mirror field lens there are two electrostatic and two magnetic multipoles used to adjust the tilt of the incoming and outgoing rays relative to the mirror and the beam splitter. Furthermore they can be used to correct for stigmatism in the image.

After a second passage through the beam splitter, the transfer optics, composed of 5 electrostatic lenses and a contrast aperture, is used to place the image and diffraction planes in two fixed positions at the entry of the energy filter. First the diffraction plane is fixed inside the contrast aperture and the lens T5, so that the latter can be used to adjust the position of the image plane, which needs to be 95 mm after it. Besides fixing

the position of the diffraction and imaging planes, the transfer optics can introduce a magnification from 2 to 44. Furthermore the diffraction plane can be imaged by inversion, inside the transfer optics, of the image position and diffraction planes. In such way it is possible to achieve PED (Photo Electron Diffraction) or LEED (Low Energy Electron Diffraction).

The Ω-shaped energy filter is a magnetic imaging energy filter with imaging aberrations that can be compensated for, up to second order, by use of six hexapoles and a dodecapole. The fixed entrance imaging and diffraction planes are transferred to the achromatic image plane after the filter without magnification (magnification = 1). The dispersion of the energy filter is 35 μm/eV. The smallest exit slit available is 3.5 μm wide thus reaching an energy resolution of $\delta E = 0.1$ eV.

The projection optics, composed of three electrostatic lenses, is used to image either the achromatic image plane, leading to energy filtered imaging when an exit slit is used, or the energy dispersive plane (spectrum imaging). In the latter mode a linear spectrum of about 35 eV can be imaged at once. Thereafter, the beam reaches a 2D detector system. Two interchangeable systems can be used. The first consists of channel plates followed by a phosphorescent screen. This allows video-rate image acquisition and is particularly useful for the alignment of the instrument. The second system has not been implemented yet and consists of a in-vacuum slow-scan CCD. This is particularly useful for high-resolution imaging with low background noise (no amplification is required).

2.3 Looking deeper inside the SMART

In this section some details of the construction of the instrument and of how these parts interact together are given.

2.3.1 Main and preparation chamber, the refocusing mirror

The sample located in the main chamber can be accessed through 8 ports in the sample plane and other 8 with a 20° angle to it as shown in figure 2.4. Of the flanges in the sample plane, six are used as view-ports, one to transfer the sample cartridge to a separately built preparation chamber, equipped with a mini-manipulator for annealing,

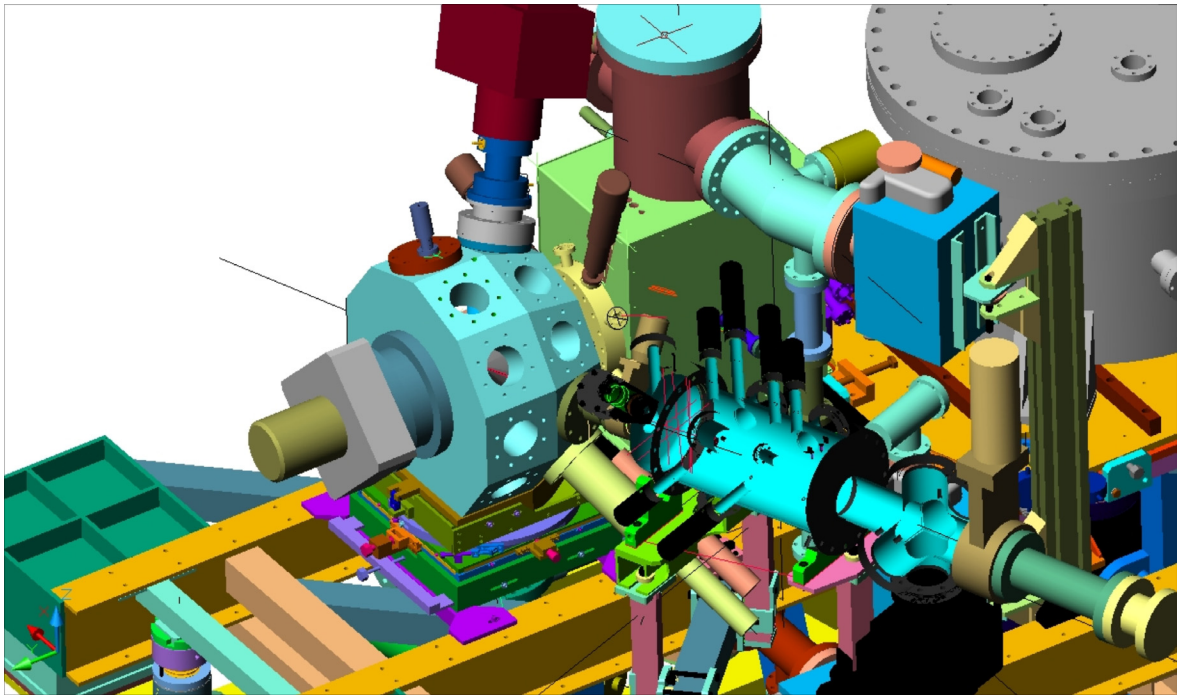

Figure 2.4: CAD drawing of main chamber and refocusing mirror. Adapted from [25].

a sputter gun, and one which is used as shutter for the neighboring UV-short-arc source. In the preparation chamber, common sample preparation procedures, such as annealing, argon sputtering and gas dosing through a leak-valve, can be undertaken. A load-lock system can be used for quick sample exchange. Further details of the construction can be found in [26].

Of the 20° tilted ports two are used for the X-Ray and UV-illumination. The former is connected to a chamber with a toroidal refocusing x-ray mirror whose mounting stage has been designed and assembled by *U. Groh* [26]. Six degrees of freedom allow the adjustment of the toroidal mirror position and orientation to properly focus the x-rays in both, horizontal and vertical directions. For the UV-illumination a laboratory Hg-short arc lamp is mounted, that has a maximum photon energy of 4.9 eV, and it is focused on the sample by in-vacuum fused-quartz silica optics which reach a maximum flux density that is 30 times higher than that of conventional UV-light sources. Three other ports are connected to evaporators for NTCDA, PTCDA and Cu deposition.

The sample is located on a high stability and high precision manipulator which

allows movements along two perpendicular axes of ±5 mm in the sample plane and 50 mm travel along the manipulator axis for adjustment of the sample-objective lens distance. Furthermore the sample's tilt can be regulated with two perpendicular eucentric tilt regulators (such that the imaged region is not changed upon adjustment) for angles up to ±2° [27]. The exchangeable sample cartridges with integrated electron bombardment heating allow reaching *in-situ* condition temperatures of 1800 K or 2300 K for flash, and with liquid nitrogen cooling down to 150 K. The temperature is measured with a tungsten/rhenium alloy (W-5%Re vs. W-26%Re) thermocouple.

The objective lens is an electrostatic immersion lens (also known as cathode lens) with a superimposed magnetic field (therefore electromagnetic lens), stigmators and deflection elements. The objective lens is the element that introduces the aberrations that limit the lateral resolution. Since the electron mirror is designed to compensate for these aberrations, the design of the lens was carried out following strict theoretical predictions of the introduced aberrations. Furthermore also the technical design of the lens had to deal with a high current in the magnetic coil which can result in an overheating. The lens is supplied with a highly stable water cooling system. An exchangeable protective plate is placed on the front surface toward the sample to facilitate the removal of coatings deposited during experiments.

2.3.2 The beamline

Since its arrival at BESSY II in 2001, the SMART has been always connected to one beamline but the undulator has been exchanged in the spring of 2002. The first one, active until March 2002, was the U49/1 (with 84 magnetic sections, each 49 mm long) and delivered *only* horizontally polarized light. Successively, undulator UE52, of APPLE II type (with 79 magnetic sections, each 52 mm long), has been installed delivering both elliptically and linearly polarized light. In both cases the beamline [28] uses a Plane-Grating-Mirror (PGM) monochromator (Petersen design [29]). The reason for the use of this monochromator with respect to the Focused Spherical Grating Mirror (FSGM) is that although it has a slightly lower brilliance, the freedom of choice of the c_{ff} parameter (which regulates the energy dispersion at the energy slit) combined with an almost constant relative energy resolution is of great experimental advantage.

The beamline can supply photon energies in the range from 90 to 2000 eV with a resolving power of $E/\Delta E = 12000$ and photon flux of $3 \cdot 10^{11}$ ph/s on an area of $6 \times 30\mu m^2$ at 400 eV. Details of the beamline and the construction of the refocusing optics are described elsewhere [26].

2.3.3 Electron source and illumination optics

The electron source is a Schottky field emitter [30]. This consists of a sharply pointed single crystal tungsten needle previously chemically modified with zirconium to reduce the work function. The Schottky emission occurs as electrons are thermally excited over a field-lowered potential barrier. In order to obtain high resolution images the source and illumination optics had to be redesigned. For this purpose dedicated calculations [31] have shown that a set of four lenses (one magnetic condenser and three electrostatic) would be necessary. The maximum calculated current density obtainable at the sample is so high that at 100 eV kinetic energy, a power of 400 W/mm^2 has to be dissipated by the illuminated area. For this reason apertures have been inserted to reduce the flux and improve the beam quality by reducing the illumination by angularly divergent rays.

2.3.4 The aberration corrector

The so-called tetrode mirror or aberration corrector, a picture of which is shown in the left of figure 2.5, is the most innovative part of the microscope. Its role is to introduce spherical and chromatic aberrations of the opposite sign with respect to those introduced by the objective lens. In the following a relatively easy and descriptive introduction is given on how the mirror is used to correct spherical and chromatic aberrations without entering the details of ray-tracing calculations but only exploring the results and the necessary physical background. Figures 2.6.a and 2.6.b show schematically how spherical and chromatic aberrations are introduced by a conventional lens and this effect is then compared with that of a mirror. The left side of figure 2.6.a shows the effect of spherical aberrations caused by a lens on rays having different angular divergence α. For high values of α, the back focal plane is formed at a

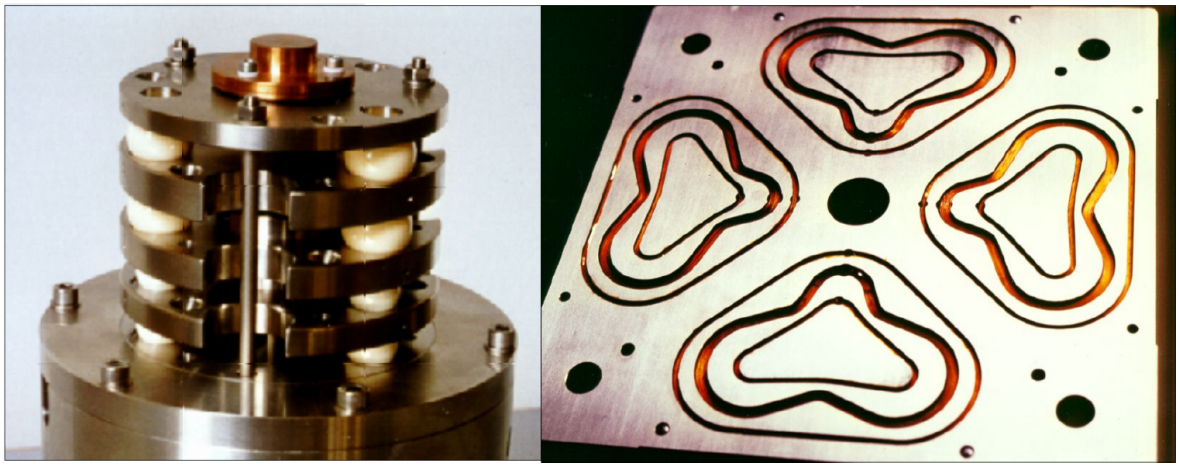

Figure 2.5: Photo of the aberration corrector (left) and the pole-plates of the beam splitter (right). The four electrodes of the mirror are recognizable as metal disks and are separated by insulating white ceramic spheres. The top electrode and the bottom plate are on ground potential. The pole-plate of the beam splitter shows three coils in each of the four sectors. The outer coils are for fine adjustment.

shorter distance from the lens. The effect of the mirror, on the right side of figure 2.6.a, can be just the opposite and can thus be used to compensate. A similar situation is presented in figure 2.6.b which depicts two rays with the same angular divergence but different kinetic energy (represented in the figure with different colors)[2]. While for the lens the distance to the back focal plane of the ray with higher kinetic energy (blue in the image) is higher than that with lower energy, the opposite happens for the mirror. The effect appears to be very similar to that experienced by rays with different kinetic energies interacting with the potential of the lens, but the main difference here is that electrons with higher kinetic energies will travel further inside the mirror and interact with more equipotential surfaces, showed in figure 2.6.c, whose cylindrically symmetric curvature profile changes along the z-axis.

The mirror is then tuned, to reproduce different spherical and chromatic aberrations according to the experimental conditions (mainly kinetic energy of the electrons), by

[2]For the discussion on the chromatic aberrations, the divergence angle α is assumed to be constant. It must be pointed out that the divergency, high α, will increase the effect of chromatic aberrations because the chromatic aberration coefficient is $\propto \alpha\Delta E$.

varying the three potentials U_0 to U_2. For a fixed electron kinetic energy, the changes can affect the curvature of the relevant equipotential surfaces so that electrons at different angular divergences reflect back at the appropriate distances, to obtain the effect depicted in figure 2.6.a. In the same way, the degree of curvature modification deeper in the mirror can be adjusted to compensate for the chromatic aberrations.

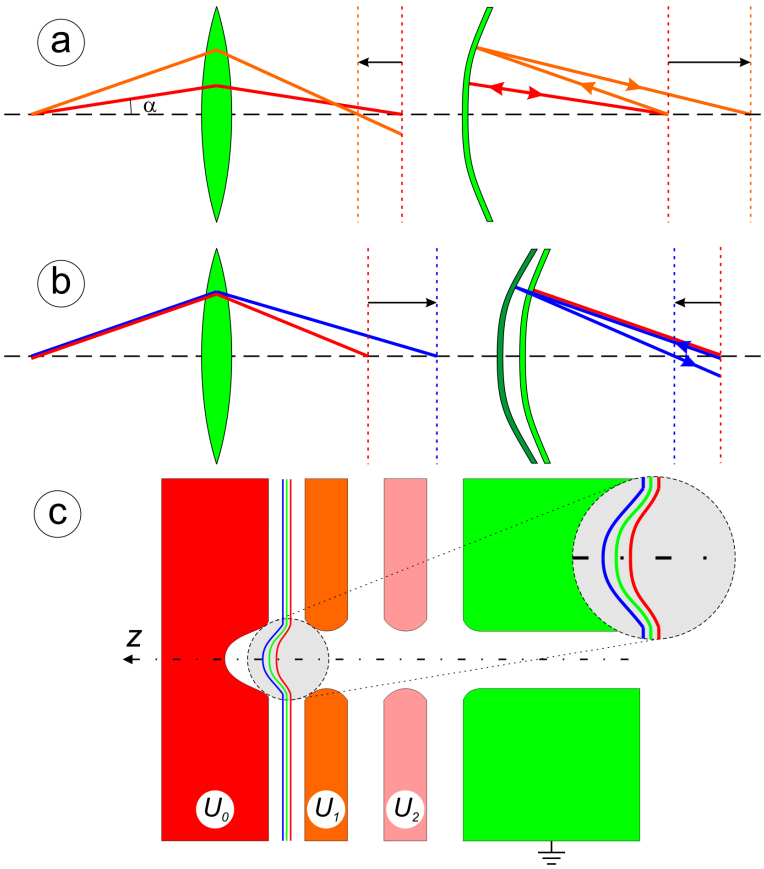

Figure 2.6: (a) effect of spherical aberrations on rays with different divergence angle α with a lens (left side) and a mirror (right side). (b) effect of chromatic aberrations on rays with different energy (red = 15 keV, blue > 15 keV) with a lens (left side) and a mirror (right side). (c) Slice cut through the axis of the mirror showing the equipotential lines (surfaces in 3D) responsible for the correction of spherical and chromatic aberrations.

The range of spherical and chromatic aberration coefficients that can be compensated by the mirror is shown in figure 2.7 (adapted from [32]) contained in the yellow region. The lines represent settings with fixed electrical field at the sample surface

of 5 kV/mm, 1 kV/mm and 0 kV/mm (field free mode can only be used for kinetic energies above 500 eV) for the green, red and blue line, respectively. Along each line the electron kinetic energy is given.

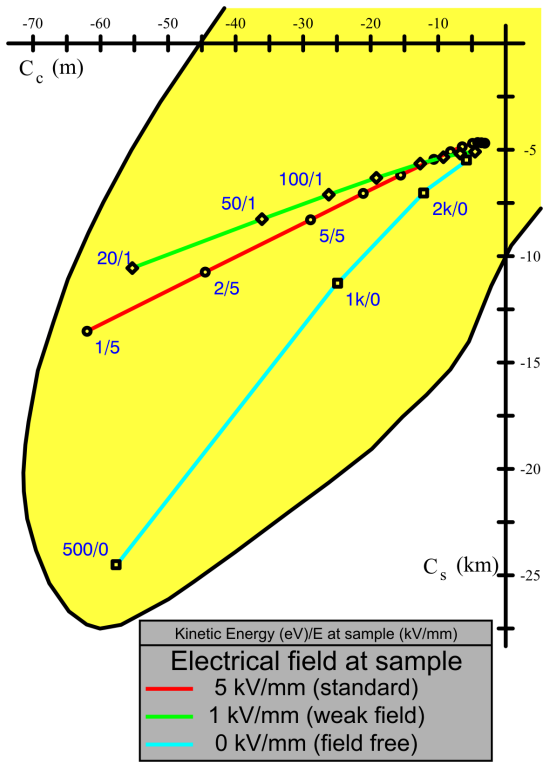

Figure 2.7: Aberration coefficients of the objective lens for different start voltages (along each line) and different electric fields at the sample (indicated by the colored lines). The yellow contour shows the region of aberration coefficients that can be compensated by the mirror (the mirror aberration coefficients would have the opposite sign).

In sub-section 4.1.1, on page 33, examples will show how aberrations, both spherical and chromatic, have been proven to be corrected.

2.3.5 The main imaging column: the transfer optics

The role of the transfer optics is to magnify the image and appropriately place the image and the back focal plane at the entrance of the energy filter. The back focal plane has to be kept all the time (except when diffraction imaging is performed) inside the contrast aperture. The magnification of the intermediate image found in front of T1

(see figure 2.3) at the exit of the beam splitter can be of a factor 2 to 44. The distance of the image plane from the back focal plane, a parameter known as the Helmholtz length, at the entrance of the energy filter is a fixed parameter of a spectrometer and in our case it is 95 mm.

For these purposes the transfer optics is composed of 5 electrostatic lenses (T1-T5), three electrostatic double deflectors (D1-D3) and a contrast aperture (with diameters from 3 mm to 20 μm) as shown in figure 2.3.

The intermediate image formed at the exit of the beam splitter is in the focal plane of T1. In such way the position of the back focal plane is transferred in the location of the plane of the contrast aperture, exactly between T1 and T2. The role of the following two lenses, T2 and T3, is mainly to set the magnification. Then T4 is used to adjust the position of the back focal plane which is the entrance plane of the energy filter at a distance of 95 mm in front of the field aperture. This position is located just inside T5 so that T5 can then be used to adjust the position of the image plane in the energy filter. In this way the contrast aperture, which defines the extensions of the back focal plane in T5, is used as a virtual entrance aperture for the energy filter.

2.3.6 The energy filter

The imaging energy filter generates a 1:1 stigmatic image of the source image in the energy dispersive plane 90 mm after the last dipole. In the dispersive plane electrons with different kinetic energies will be focussed with different horizontal displacements (in the plane of figure 2.3) away from the optical axis. Therefore there is a spectrum in this plane which has a dispersion of 35 μm/eV; in this plane the exit slit is placed. The achromatic image plane is situated 5 mm from the front of the last dipole, i.e. inside the dipole. Electrons with different kinetic energies will generate identical images in the achromatic image plane. It is this plane that is normally imaged by the projection optics.

In order to account for the distortions introduced in the image by the non-spherically symmetric (dipole) magnetic filed, magnetic multipoles are used. These are placed inside the filter and can correct for aberrations and distortions in the image plane as well as in the diffraction plane. The theoretically predicted energy resolution of the

energy filter is of 100 meV with a 600 μm field of view at the entrance plane [33]. If the path energy of 15 keV is taken into account, the resolving power of this analyzer gives an extremely high value of $1.5 \cdot 10^5$.

2.3.7 The projection optics and the 2d detection system

The projection optics further magnifies the image at the exit of the energy filter, in the achromatic image plane, onto the 2d detection system. The optics itself can be used in different modes. The first lens, P1, can transfer the image into one of the following lenses, P2 or P3, and different magnifications up to 160:1 are obtained.

Alternatively, the projection optics can be used for spectroscopic imaging. In this case P1 images the energy dispersive plane directly onto the detector and the other two lenses, P2 and P3, are not used. In such a mode, a spectrum of circa 35 eV can be imaged at once. Furthermore, using the field aperture, which is placed in the image plane at the entrance of the energy filter, a specific region of the sample can be selected with an area down to 25 nm^2 enabling nano-spectroscopy.